Renewable Energy 172 (2021) 1351–1364

Contents lists available at ScienceDirect

Renewable Energy

journal homepage: www.elsevier.com/locate/renene

Carbon nanotube-graphene supported bimetallic electrocatalyst for direct borohydride hydrogen peroxide fuel cells

Arife Uzundurukan [a], Elif Seda Akça [b], Yağmur Budak [c], Yılser Devrim [d, *]

[a] Department of Mechanical Engineering, Université de Sherbrooke, 2500 Boulevard de L'Université, Sherbrooke, QC, J1K 2R1, Canada
[b] Izmir Institute of Technology, Department of Energy Systems Engineering, İzmir, Turkey
[c] Atılım University, Department of Mechanical Engineering, İncek, Ankara, 06836, Turkey
[d] Atılım University, Department of Energy Systems Engineering, İncek, Ankara, 06836, Turkey

ARTICLE INFO

Article history:
Received 26 April 2020
Received in revised form
14 October 2020
Accepted 1 December 2020
Available online 9 December 2020

Keywords:
Direct borohydride-hydrogen peroxide fuel cell
Bimetallic catalyst
Hydrogen peroxide
Sodium borohydride
Liquid fuels fuel cell

ABSTRACT

At present study, carbon nanotube-graphene (CNT-G) supported PtAu, Au and Pt catalysts were prepared by microwave-assisted synthesis method to investigate the direct liquid-fed sodium borohydride/hydrogen peroxide ($NaBH_4/H_2O_2$) fuel cell performance. Prepared catalysts were characterized by TGA, XRD, TEM, ICP-OES, cyclic voltammetry and rotating disc electrode (RDE) voltammetry. The catalysts were tested in a single $NaBH_4/H_2O_2$ fuel cell with 25 cm^2 active area to evaluate fuel cell performance. The effects of temperature and fuel concentration on fuel cell performance were examined to observed best operating conditions. As a result of direct $NaBH_4/H_2O_2$ fuel cell experiments, maximum power densities of 139 mW/cm^2, 125 mW/cm^2 and 113 mW/cm^2 were obtained for PtAu/CNT-G, Au/CNT-G and Pt/CNT-G catalysts, respectively. PtAu/CNT-G catalyst showed the enhanced $NaBH_4/H_2O_2$ fuel cell performance, which was higher than the Pt/CNT-G catalyst and Au/CNT-G catalyst at 50 °C. The enhanced $NaBH_4/H_2O_2$ performance can be attributed to synergistic effects between Pt and Au particles on CNT-G support providing a better catalyst utilization and interaction. These results suggest that the prepared PtAu/CNT-G catalyst is a promising anode catalyst for $NaBH_4/H_2O_2$ fuel cell application.

1. Introduction

Proton exchange membrane fuel cell (PEMFC) using high purity hydrogen gas as fuel is not widely commercialized due to the limitations imposed by the transport and storage safety of hydrogen gas. Therefore, liquid fuels such as methanol, ethanol, propanol, ethylene glycol and diethyl ether offer better safety in transportation and storage for PEMFC [1,2]. Direct liquid sodium borohydride ($NaBH_4$) fuel cells have advantages over other gas-fed fuel cells due to the high theoretical cell voltage, high power density, high energy density, easy refueling ability, harmless to the environment, quick response properties and simple system design [3]. In addition to the studies on fuel cell fuels, researches on liquid oxidants have increased in recent years. Hydrogen peroxide (H_2O_2) is well-known oxidizer used in the application of air independent propulsion (AIP). Especially, H_2O_2 based fuel cell is an ideal solution for space or submarine power applications [4]. H_2O_2 is the environmental friendly chemical, it can be produced in high volume with very low cost, and it is easy to store and transport [5]. Since H_2O_2 reduction in fuel cells has a lower activation barrier and faster kinetics compared to four-electron oxygen (O_2) reduction, it is easier to reach higher power densities than H_2—O_2 fuel cells [6]. The theoretical cell voltage of direct liquid feed $NaBH_4/H_2O_2$fuel cells can increase up to 3 V which exceeds cell voltages of H_2—O_2 fuel cells. In this way, fuel cells can be operated at higher voltage than pure H_2 feed PEMFC [7]. However, there are still some basic problems in $NaBH_4/H_2O_2$ fuel cell.

The complete oxidation of and reduction of takes place anode and cathode side is given Equation (1) and Equation (2), respectively [8].

$$BH_4^- + 8OH^- \rightarrow BO_2^- + 6H_2O + 8e^- \quad (1)$$

$$H_2O_2 + 2H^+ + 2e^- \rightarrow 2\,H_2O \quad (2)$$

However, in actual applications there are undesirable reactions that compete at each electrode. If the borohydride hydrolysis reaction occurs less than eight electrons are exchanged, and low cell performance is achieved (Equation (3) and Equation (4)) [9].

* Corresponding author.
E-mail address: yilser.devrim@atilim.edu.tr (Y. Devrim).

https://doi.org/10.1016/j.renene.2020.12.003
0960-1481/

$$BH_4^- + H_2O \rightarrow BH_3OH^- + H_2 \quad (3)$$

$$BH_3OH^- + H_2O \rightarrow BO_2^- + 3H_2 \quad (4)$$

Additionally, the released H_2 can adsorb to the catalyst surface. As a result, H_2 can prevent ion transport in the active areas of the catalyst and reduce electrode activity.

One of the important parameters to overcome the limitations of the $NaBH_4/H_2O_2$ fuel cell is to develop suitable anode catalyst that is electrochemically active for borohydride oxidation and is not suitable for hydrolysis of borohydride to H_2 [10]. Catalyst such as Pt [11], Pd [12], Au [13–15], Ag [16], Co [17], Ni [18] and Os [19] have been extensively investigated for $NaBH_4$ electro-oxidation. The use of noble metals is more advantageous because of their high catalytic activity against $NaBH_4$ oxidation. Among the noble metals, Pt is the best choice with activity compared to others. Oh et al. [20] investigated the effect of various catalysts such as Pt, Au, Pd, Ni, and Cu supported on multi-walled carbon nanotubes on $NaBH_4$ oxidation and H_2O_2 reduction and compared their activity by fuel cell performance tests. The catalytic activity of the anode catalysts on $NaBH_4$ decomposition was observed in the following order: Pt > Pd > Ni > Cu > Au. However, carbon supported Pt has low performance in $NaBH_4/H_2O_2$ fuel cell applications. Oxidation of $NaBH_4$ ions in the presence of Pt catalyst is complicated by oxidation of the intermediates and hydrolysis reaction [21]. To improve the performance of $NaBH_4/H_2O_2$ fuel cell, the development of bimetallic Pt–M (M = Au, Pd, Ru, Bi, etc.) catalysts has been recognized as an effective strategy. Among them Au is a good candidate for preparing Pt based bimetallic catalyst due to the efficient $NaBH_4$ oxidation [22,23]. Synergic interaction between Pt-based bimetallic nanoparticles such as PtAu have been documented for different application [24–26]. Nonetheless, Carbon Nanotube-Graphene (CNT-G) supported PtAu bimetallic catalysts have not been investigated for $NaBH_4/H_2O_2$ fuel cells.

One of the important points in the development of fuel cell catalyst is the use of suitable catalyst support material. The support materials used in the fuel cell must have high electrochemical stability, large surface area and corrosion resistance [27,28]. Various types of carbon based materials have been used as supports in PEMFCs including carbon black (CB) [29,30], graphene [31,32], graphene oxide [33,34], carbon nanotubes (CNTs) [35–38], carbon aerogel (CA) [39] and etc. Among them, there are several advantages in using graphene as catalyst supports due to its structural properties, high surface areas and superior properties [40–44]. Ishikawa et al. [28] showed that PtAu/graphene exhibited enhanced electrocatalytic activity for formic acid oxidation compared to Pt/C catalyst. However, when graphene is used as support material, the problem of re-stacking of graphene layers is encountered. This problem affects the distribution of the catalyst on the support material and its performance in the fuel cell applications [45]. One of the promising solutions is to prevent the re-stacking of the graphene layers with another support material used with graphene. The hybrid support materials are more effective than single-supported catalysts or composite catalysts due to the high active area. Alpaydin et al. [46] investigated the effect of CNT and graphene hybrid catalyst supports on the performance on PEMFC and the results showed that the CNT and graphene hybrid catalyst is a better support material than the carbon black. Inclusion of CNT in graphene decreases the adhesion of graphene layers by increasing π - π interactions and consequently helps increase the electrocatalytic activity by providing more dispersed Pt nanoparticles to be loaded on the support material. Therefore, the use of new catalyst and electrode systems for $NaBH_4/H_2O_2$ fuel cell is the most critical factor affecting the cell performance and thus the final conceptual design. In this regard, it is expected that graphene based composite material may be used as a support material for the next generation catalysts in fuel cells.

Considering all these approaches, in this study, CNT-G hybrid support material was selected to be used as support material for Pt and Au based bimetallic catalyst for the $NaBH_4/H_2O_2$ fuel cell application. To our knowledge, no studies have been conducted to investigate the use of CNT-G as a support material for the PtAu bimetallic catalyst for direct feed $NaBH_4/H_2O_2$ fuel cell application. The CNT-G supported catalysts were characterized by XRD, TGA, TEM, ICP-MS and their electro-catalytic behavior was evaluated using cyclic voltammetry and RDE voltammetry. To observe the suitability of the catalysts, they were evaluated by direct liquid feed $NaBH_4/H_2O_2$ fuel cell tests.

2. Experimental

2.1. Materials

$H_2PtCl_6 \cdot 6H_2O$ and $HAuCl_4 \cdot 3H_2O$ precursors were purchased from Sigma-Aldrich ® and used as received. CNT-G hybrid support material was purchased from Nanografi (Turkey). H_2O_2 and $NaBH_4$ were purchased from Sigma-Aldrich (USA). Since both chemicals and solvents have high-grade reagents, they were used without further purification. The commercial carbon paper Gas Diffusion Layer (GDL) was supplied from Freudenberg (Germany). The commercially available Pt/C (40 wt % Pt, Johnson Matthey, UK) catalyst was used as cathode catalyst. Nafion® 115 membrane was purchased from Fuel Cell Store (USA). Nafion solution (LIQUION™ Solution, 15 wt %) was obtained from Ion Power Inc. (Delaware, USA). High-purity N_2 gas was supplied from Linde gas (Turkey).

2.2. Catalyst preparation

PtAu (1:1)/CNT-G catalyst with 30 wt % metal loading was prepared according to the $NaBH_4$ chemical reduction method [47]. Firstly, 25 mg of CNT-G was dispersed in 10 mL DI water by ultrasonic mixing for 10 min. Simultaneously, 14 mg of $H_2PtCl_6 \cdot 6H_2O$ was dispersed in 15 mL DI water for 10 min by ultrasonic bath. Then, these two solutions were stirred ultrasonically for 15 min. 3 mL of $NaBH_4$ was added to the resulting solution and stirring was continued for a further 20 min. After this step, 10.65 mg of $HAuCl_4 \cdot 3H_2O$ was added to the solution and stirring was continued at room temperature for 20 min. The resulting mixture was filtered, washed with deionized water and dried in an oven at 80 °C during overnight.

As a typical process for the synthesis of Au/CNT-G catalyst with the Au loading of 30 wt %, 25 mg CNT-G was dispersed in a mixture of 10 mL DI water and with ultrasonic bath for 10 min. After 10 min, the solution was added into the 3 mL 0.1 M $NaBH_4$ solution and ultrasonic treatment was applied for 30 min. Then 22 mg $HAuCl_4 \cdot 3H_2O$ was added in this solution. The resultant mixture was mixed ultrasonically during 20 min at room temperature. Finally, the resulting mixture was filtered, the solids washed with distilled water and oven dried at 80 °C overnight. For comparison, Pt/CNT-G catalyst was prepared by microwave synthesis according to our previous study [45].

2.3. Characterization

X-ray diffraction (XRD) patterns were recorded on a Rigaku Ultima-IV device using Cu $K\alpha_1$ (λ = 1.5406 °A) as the radiation source which is operating at 20–60 kV and 2–60 mA. The thermal gravimetric analysis of the catalysts were studied by Thermal Analyzer (Perkin Elmer Pyris 1) in the range of 100–900 °C with a heating rate of 10 °C/min under the air. The homogeneity and size

of the metal particles over the supports were characterized by JEOL 2100 JEM TEM instrument working at high-resolution (HR) mode. The metal contents of the catalyst were determined by Inductively Coupled Plasma Optical Emission Spectroscopy (ICP-OES, PerkinElmer Optima 4300DV).

2.4. Electrochemical characterization

The prepared catalysts were electrochemically characterized in a standard three-electrode with a potentiostat (Wonatech ZIVE-SP2) at room temperature. A glassy carbon (GC) disk with an area of 0.07 cm^2 was used as working electrode. Ag/AgCl filled with saturated KCl solution and a graphite rod served as reference and counter electrodes, respectively. The catalyst ink for working electrode was prepared by mixing the required amounts of the catalysts with deionized water, 1,2-propandiol, and 15% Nafion® solution. The ink was mixed with ultrasonic bath, then 2 μL ink loaded on the working electrode at the desired catalyst loading (21 μg/cm^2) and dried in air overnight. Prior to the experiments the electrolyte solution was purged for 15 min with N_2 to remove any O_2. The cyclic voltammetry experiments were performed at room temperature with 100 mV/s between −0.25–1.2 V in 0.1 M $HClO_4$ solution. Electrochemical active surface area (ECSA) of the catalysts were determined before and after the degradation tests [48]. To determine the borohydride electro oxidation reaction activity, cyclic voltammetry (CV) curves were plotted at a potential range from −1.2 to 0.6 V in a solution of containing 0.03 M $NaBH_4$ solution in 2 M NaOH at 25 °C with a scan rate of 0.1 V/s. RDE technique was applied to determine the BOR kinetics of the prepared catalysts. RDE voltammetry experiments were performed at a 20 mV/s potential sweep rate in 0.12 M $NaBH_4$ + 2 M NaOH solution with different rotation rates.

2.5. Performance tests

The catalysts were used at the anode side of the direct $NaBH_4$/H_2O_2 fuel cell. The commercial Pt/C catalyst was selected as cathode side catalyst. The catalyst ink was composed of 70 wt % catalyst and 30 wt % Nafion (on dry basis) in a solution of 1:7 ratio of water:2-propanol. The catalyst ink was sprayed onto the gas diffusion layer at 80 °C by the Sono-Tek 'Exacta-coat' ultrasonic spray coating instrument to prepare the gas diffusion electrodes (GDE) with 0.5 mg/cm^2 catalyst loading and 25 cm^2 active area [49]. Finally, MEA was prepared by pressing these GDEs onto the Nafion 115 membrane at 130 °C, 688 N/cm^2 for 3 min [49].

Scheme 1 shows the direct $NaBH_4$/H_2O_2 feed fuel cell test station flow scheme. The flow channel of the anode and cathode side was serpentine type. Sodium hydroxide (NaOH) and hydrochloric acid (HCl) were used for the stabilization of the fuels. The anode side reactant and cathode side oxidant were composed of 2 M $NaBH_4$ in 6 M NaOH and 2 M H_2O_2 in 1 M HCl, respectively. The fuel and oxidant tanks were stored in special containers equipped with temperature control. Each fuel was supplied at a rate of 10 mL/min. The fuel cell was operated at 1 V until it came to steady state. After steady state was achieved, starting with the OCV value, the current-voltage data were logged by changing the current set of the electronic load. The current and voltage values were monitored and logged throughout the operation with test station software.

3. Result and discussion

3.1. Characterization of CNT-G supported catalysts

Thermal gravimetric analysis (TGA) of the catalysts were performed to identify the thermal behavior of the catalysts. As seen from Fig. 1 the CNT-G support was completely oxidized and evaporated from the sample and the weight loss was measured. The first loss region between 100 and 200 °C could be related to the elimination of volatile materials. The second weight loss between 200 and 400 °C was explained by the decomposition of carboxyl and hydroxyl groups fixed on the CNT surface. The weight loss was very profound from ~400 to 650 °C. After the loss of carbon support, the steady value of weight in TGA plot indicates the weight percentage of metal present in the catalyst. TGA results in air atmosphere showed that the metal loading over the CNT-G were 30, 26 wt % and 25% for Au/CNT-G, PtAu/CNT-G and Pt/CNT-G catalysts, respectively. The metal content of the prepared catalysts was also confirmed by ICP-OES analysis.

XRD patterns of the prepared catalysts are given in Fig. 2. In all diffractograms can be clearly seen a broad peak at about 25.7° associated with the CNT-G support [22,50]. The X-ray diffraction measurements for Au/CNT-G, PtAu/CNT-G electro catalysts showed five peaks, which were associated with the planes of the face-centered cubic (fcc) structure characteristic of Au. For Au/CNT-G electro catalyst it was observed five peaks at approximately 2θ = 38.11°, 44.30°, and 64.55°, 77.57° and 81.84° which were associated with the (111), (200), (220), (311) and (222) planes, respectively, of the face-centered cubic (fcc) structure characteristic of Au and Au alloys. Au fcc peaks appeared at 38.09° for (111), 44.35° for (200), 64.56° for (220), 77.47° for (311) and 81.77° for (222) planes for PtAu/CNT-G catalyst. For PtAu/CNT-G electrocatalysts the diffraction peaks of the fcc phase were slightly shifted compared to Au/CNT-G electrocatalyst, which indicates some lattice expansion and that part of Au atoms could be incorporated into the Pt lattice. The assignment of the main Pt diffraction peaks at 39.81° (111), 46.15° (200) and 67.37° (220) reveal that Pt was crystallized in a fcc structure [51].

The mean crystallite size of the catalyst was obtained from XRD analysis using the (220) reflections of the fcc structure according to the Debye-Scherrer equation [44]:

$$D = \frac{0.9 \times \lambda}{B \times cos\theta} \quad (5)$$

where D is the crystallite size (nm), λ is the wavelength of x-ray diffraction (0.154 nm), B is a full width at half maximum (FWHM) (radians), θ is the angle at the maximum of the peak (radians). The crystallite sizes were determined as 6.94, 8.13 and 2.28 nm for PtAu/CNT-G, Au/CNT-G and Pt/CNT-G catalysts, respectively.

Fig. 3 shows the typical TEM images of the Au/CNT-G and PtAu/CNT-G catalysts. As is seen from TEM images the successful attachment of Pt and Au on the CNT-G and state of dispersion was proved. From the TEM images of PtAu/CNT-G catalyst, it was determined that Pt and Au particles were homogeneously distributed on CNT-G support material and had an average particle size of 7.05 nm. A homogeneous particle distribution was determined due to the good interaction of Pt particles with Au particles and synergistic interaction. When the TEM images of Au/CNT-G catalyst and PtAu/CNT-G catalysts were compared, it was determined that the Au/CNT-G catalyst had a bigger average particle size of 8.38 nm. The Au particles were also clearly visible without agglomeration.

The mean particle sizes of the catalysts were also calculated with Sauter mean diameter formula from TEM results [52]:

$$d_{32} = \frac{\sum_{i=1}^{n} n_i d_i^3}{\sum_{i=1}^{n} n_i d_i^2} \quad (6)$$

where ni: number of particles in size range i, di: diameter of the particle in size range i which calculated from TEM analysis. Table 1 shows the comparison of the average crystallite size, average

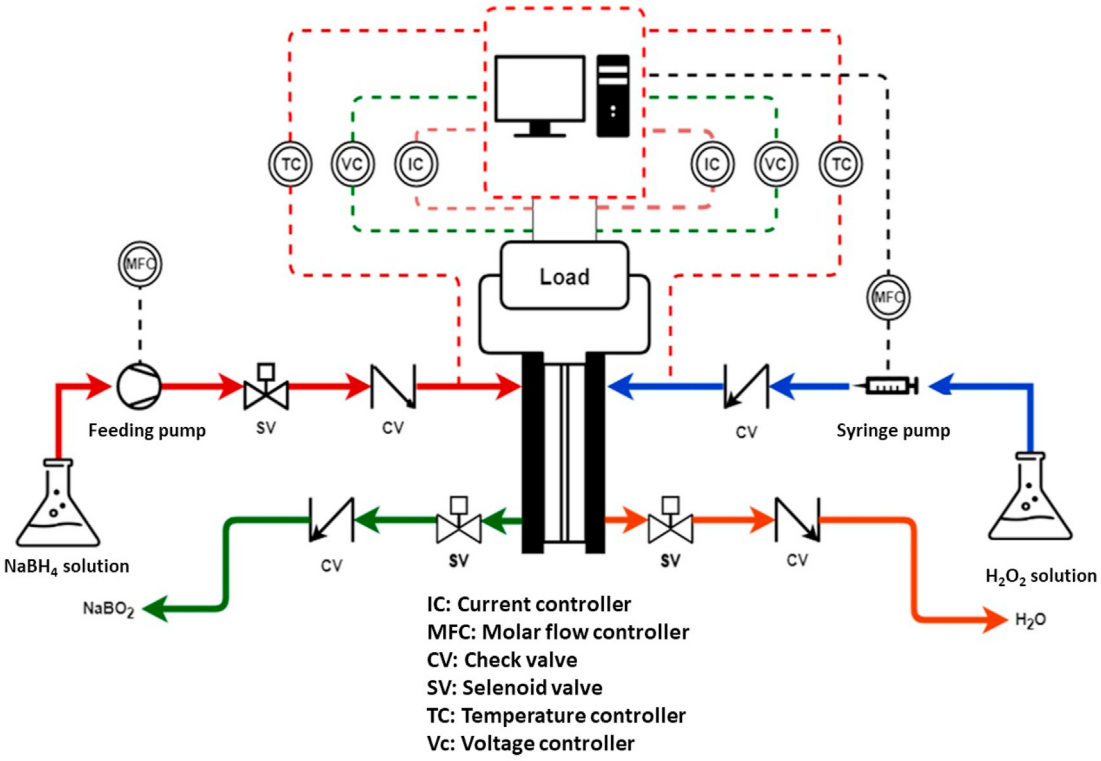

Scheme 1. Direct $NaBH_4/H_2O_2$ fuel cell test station flow scheme.

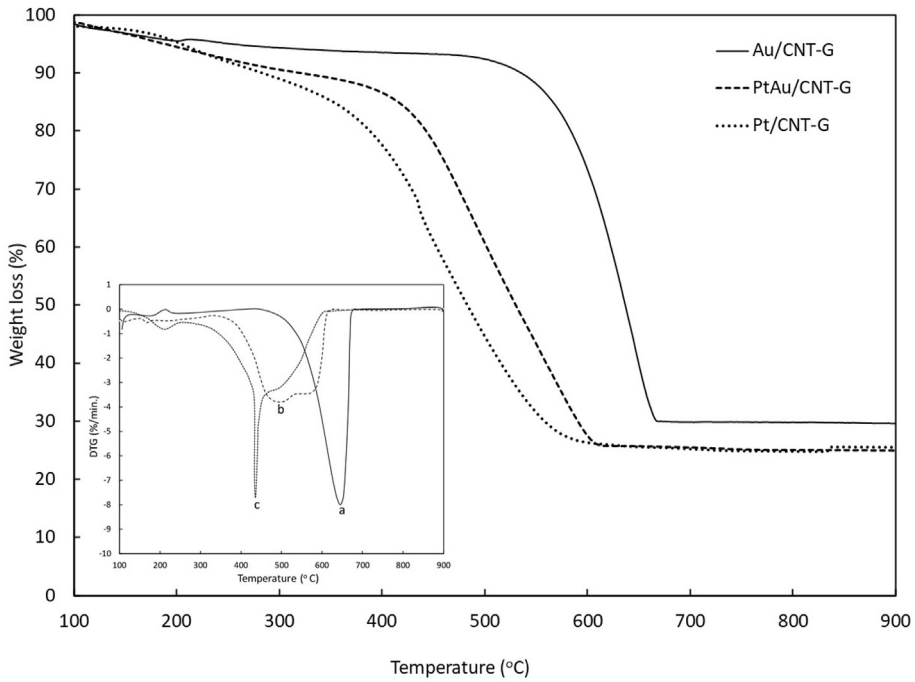

Fig. 1. TGA and DTG curves of a) Au/CNT-G, b) PtAu/CNT-G and c) Pt/CNT-G catalysts.

particle size and mean particle size of the CNT-G supported catalysts.

Fig. 4 shows the XPS spectra of the prepared catalysts. As seen from Fig. 4, Pt 4f and Au 4f XPS spectra of Pt/CNT-G catalysts represent two pairs of peaks from spin–orbital splitting of $4f_{7/2}$ and $4f_{5/2}$. The peaks at 71.7 and 74.8 eV could be assigned to Pt 4f spectra, while the peaks at 84.3 and 87.6 eV correspond to Au 4f binding energies for PtAu/CNT-G catalyst. From the XPS analysis, it could be examined that the Pt 4f binding energies was shifted to a higher peak value for the PtAu/CNT-G bimetallic catalyst as

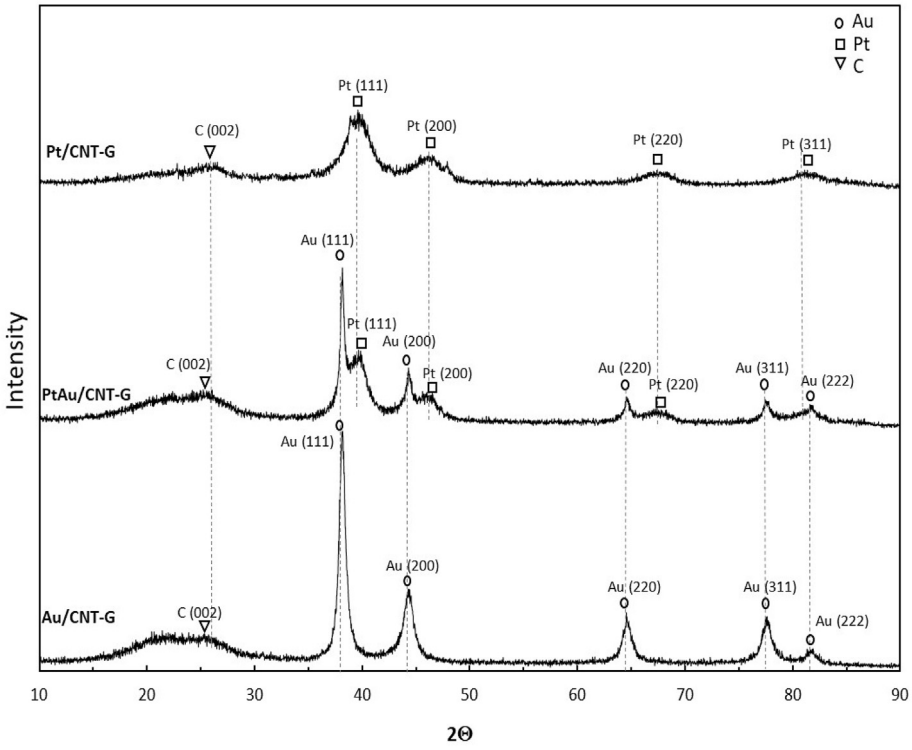

Fig. 2. XRD patterns of Pt/CNT-G, PtAu/CNT-G and Au/CNT-G catalysts.

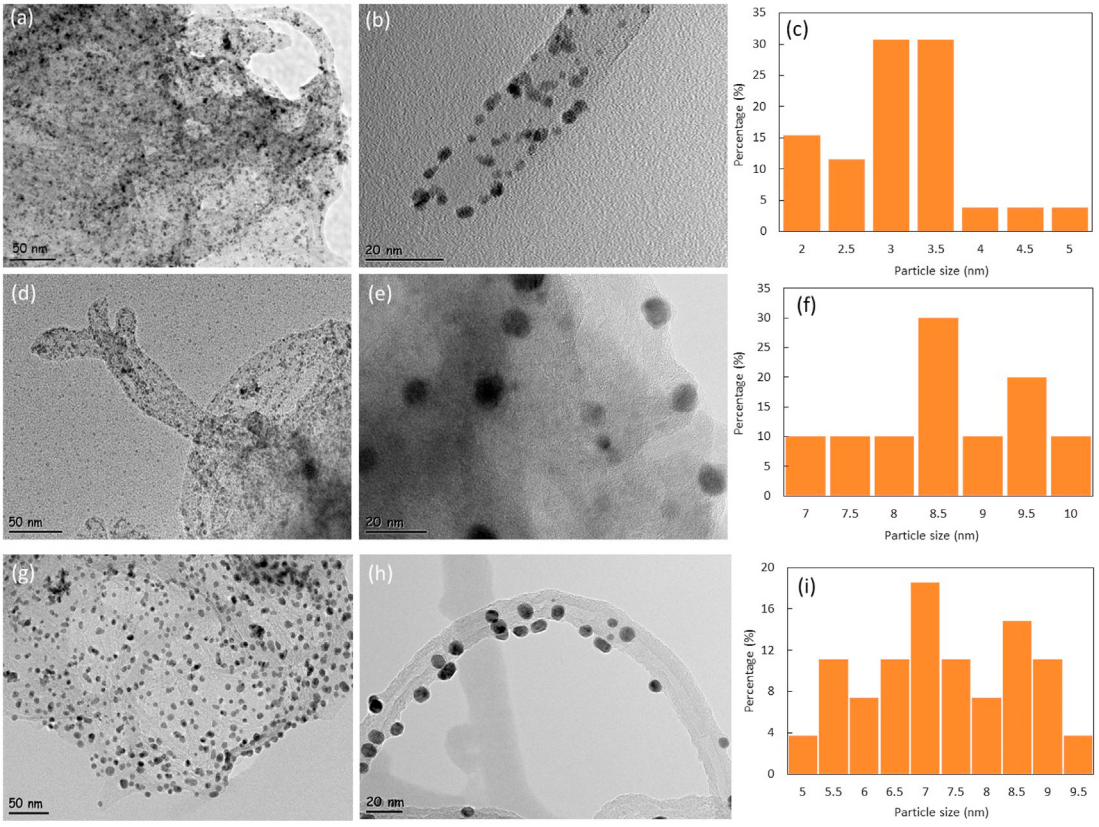

Fig. 3. TEM images and particle size histogram of a,b,c) Pt/CNT-G, d,e,f) Au/CNT-G, g,h,i) PtAu/CNT-G catalysts.

Table 1
Average crystallite size, mean and average particle size of the CNT-G supported catalysts.

Catalyst	Average crystallite size by XRD (nm)	Average particle size by TEM (nm)	Mean particle size by TEM (nm)
PtAu/CNT-G	6.94	7.05	7.47
Au/CNT-G	8.13	8.38	8.61
Pt/CNT-G	2.28	2.31	2.56

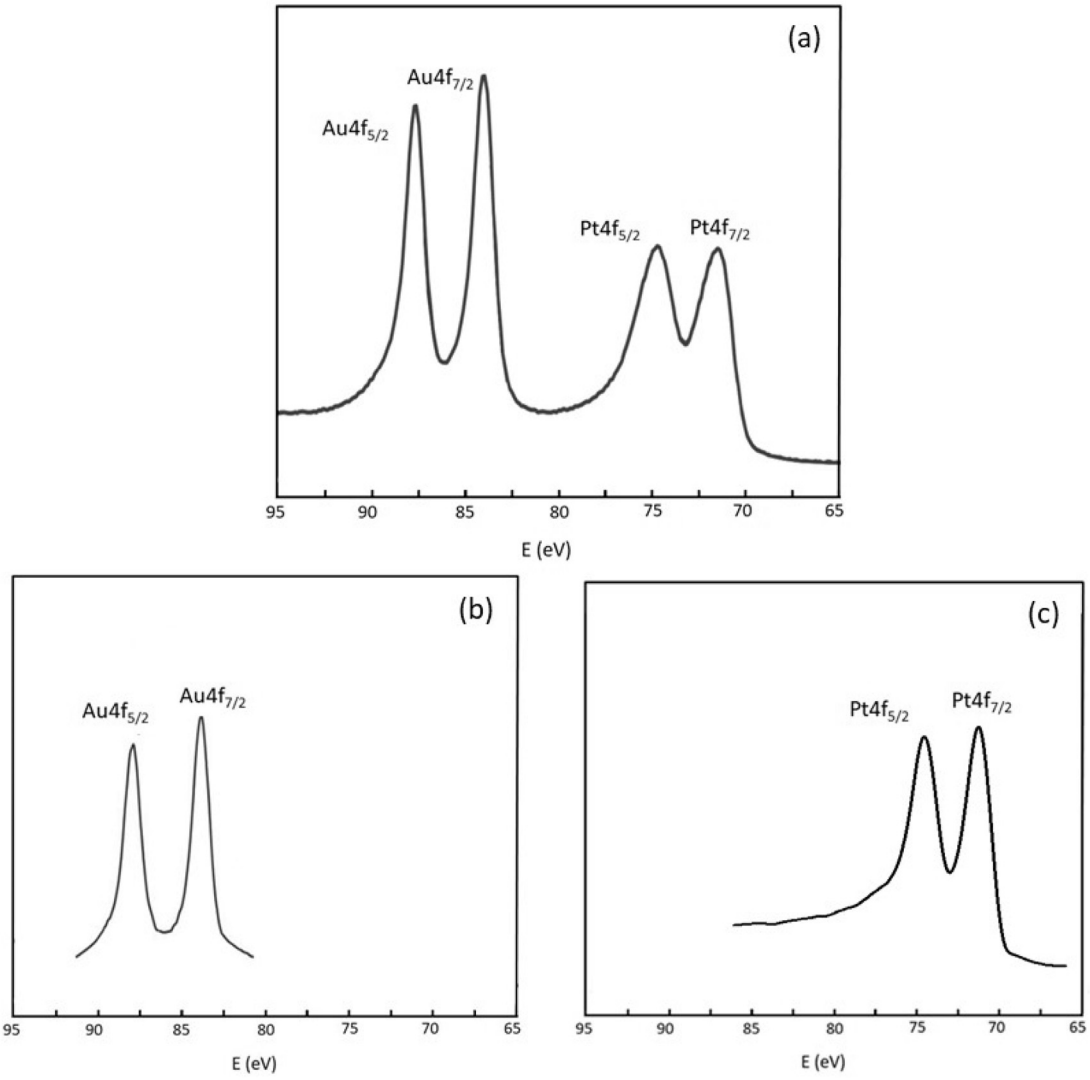

Fig. 4. XPS spectra of the a) PtAu/CNT-G, b) Au/CNT-G and c) Pt/CNT-G catalysts.

compared to the positions displayed for Pt/CNT-G catalyst. The Pt 4f spectra of the Pt/CNT-G catalyst show the usual spin–orbit splitting into a $4f_{5/2}$ peak at 74.6 eV and a $4f_{7/2}$ peak at 71.5 eV. The increase in the Pt binding energy for the PtAu/CNT-G catalyst suggests electron transfer from Pt to Au, that can be related to the electronic interaction between Pt and Au atomic orbit and alloy formation [53]. The Au^0 4f binding energies of the Au/CNT-G catalyst features the usual spin–orbit splitting into a $4f_{5/2}$ peak at 87.8 eV and a $4f_{7/2}$ peak at 84.1 eV. Similarly, Pt spectra, the Au^0 4f binding energies of Au/CNT-G catalyst shifting to a lower binding energy as compared to the position displayed for of PtAu/CNT-G catalyst.

3.2. Electrochemical measurements of the catalysts

Electrochemical measurements were performed to evaluate ECSA of catalysts. Fig. 5 displays the CV curves of the prepared catalyst. The proton desorption peaks occurred in the potential range from −0.2 to 0.1 V vs. Ag/AgCl and were used to measure the ECSA.

In the forward scan, PtAu/CNT-G and Pt/CNT-G catalysts have characteristic peaks between −0.25 and 0.1 V corresponding to H_{ad}/H_{de} followed by the "double-layer" region. The potential range from 0.1 to 0.3 V corresponds to the charge of the double layer by the oxygenated groups on the carbon support surface. The strong

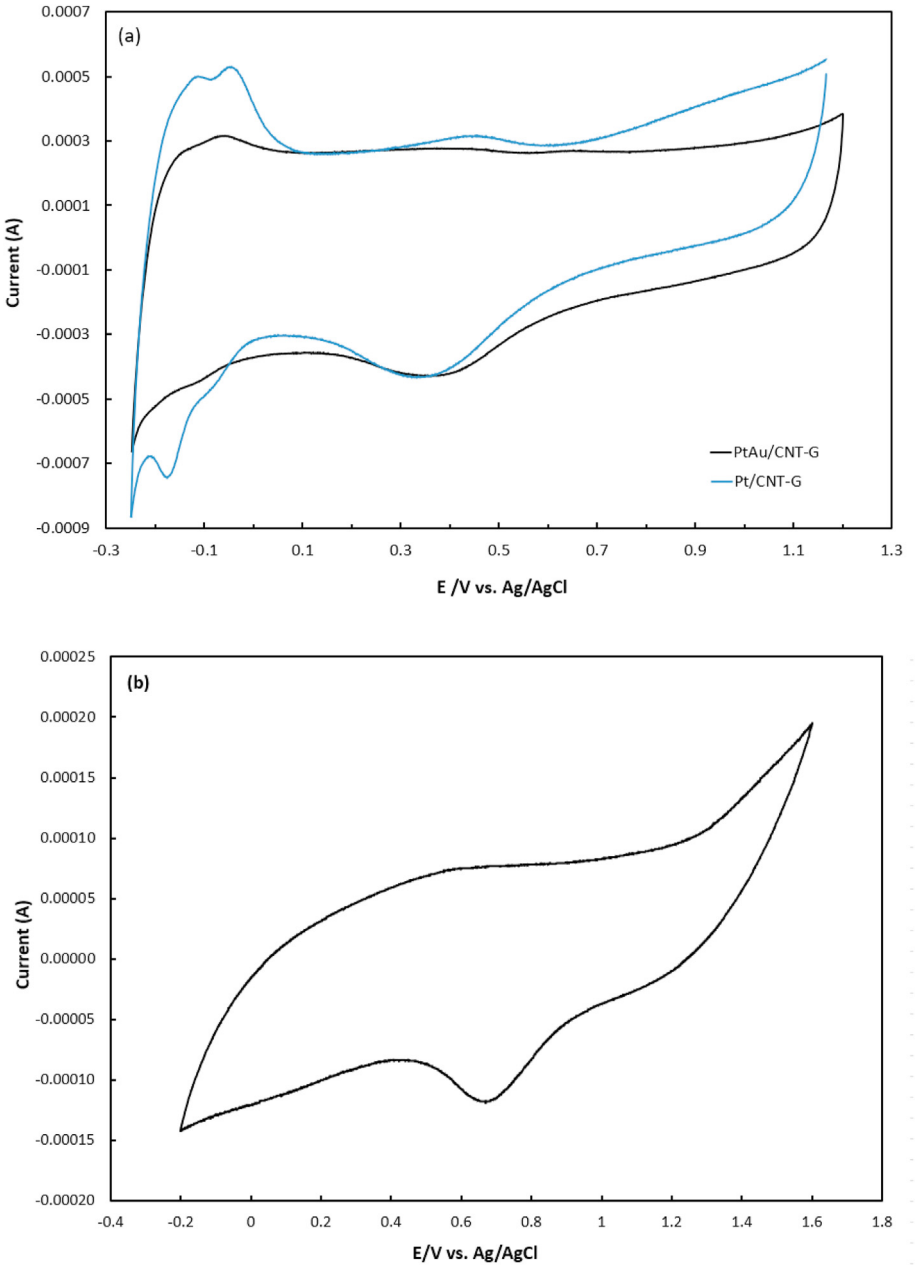

Fig. 5. CV curves of a) PtAu/CNT-G and Pt/CNT-G catalysts, b) Au/CNT-G catalyst in 0.1 M $HClO_4$ solution.

reduction peak at between 0.3 and 0.7 V vs. Ag/AgCl corresponding to formation and reduction of PtAu alloy. The small oxidation peak at 0.3 V vs. Ag/AgCl, which was attributed to the formation of gold oxides or adsorption of OH^- species on the gold surface. The oxygen reduction peak at 0.38 V in Fig. 4 clearly suggests that the PtAu/CNT-G was more electroactive towards the oxygen reduction compared with Au/CNT-G. The ECSA was calculated using Equation (7) [48].

$$ECSA\left(\frac{cm^2}{g}ofmetal\right)=\frac{Q_H\left(\frac{\mu C}{cm^2}\right)}{K\left(\frac{\mu C}{cm^2}\right)\times C_L\left(g_{metal}/m^2\right)} \quad (7)$$

Where Q_H is the charge of H_2 desorption, C_L is the catalyst loading (g/m^2) and K is the conversion factor (K_{Pt}: 210 $\mu C/cm^2$ [54] K_{Au}: 386 $\mu C/cm^2$ [55] and $K_{PtAu} = 298$ $\mu C/cm^2$). The electroactive surface area of the Pt/CNT-G, PtAu/CNT-G and Au/CNT-G catalysts were observed as 92, 25 and 6.5 m^2/g_{metal}, respectively.

Fig. 6 compares cyclic voltammograms of the PtAu/CNT-G, Au/CNT-G and Pt/CNT-G catalysts in the solution containing 0.03 M $NaBH_4$ + 2 M NaOH at room temperature and at the scan rate of 10 mV/s. From the Fig. 6, it can be seen that the CV voltammograms of Au/CNT-G, PtAu/CNT-G and Pt/CNT-G are similar, which means that these catalysts have similar reaction mechanisms for BOR electrocatalysis. Catalysis of the borohydride oxidation via the eight electrons reaction without BH_4^- hydrolysis is the most important challenge to development of electro catalysts. In the positive sweep, all catalyst show a broad oxidation peak (peak a_1), which can be attributed to the direct, potentially eight electron oxidation of BH_4^- [56]. The peak a_1 for Au/CNT-G catalyst was observed to the potential at about −0.2 to 0.2 V. According to the literature, this peak could be

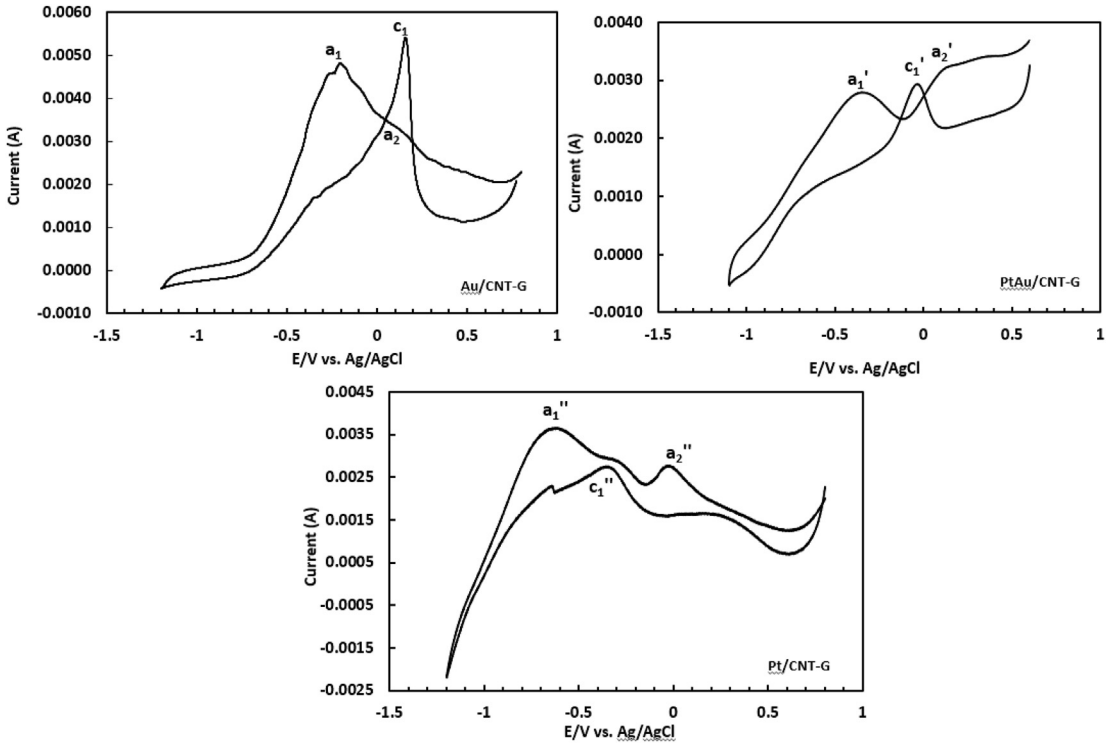

Fig. 6. Cyclic voltammograms of the PtAu/CNT-G, Au/CNT-G and Pt/CNT-G catalysts in the solution containing 0.03 M $NaBH_4$+2 M NaOH at room temperature and at the scan rate of 20 mV/s.

attributed to the direct, potentially eight-electron, oxidation of BH_4^- [57]. Compared with Au/CNT-G catalyst, peak a_1' and a_1'' of PtAu/CNT-G and Pt/CNT-G catalysts shifted to a more negative potential [58].

Fig. 6 also shows a wide oxidation peak (a_2) for Au/CNT-G catalyst, which could be due to the oxidation of reaction intermediates on the partially oxidized catalyst surface. Gyenge examined the Pt and Au electrodes for direct borohydride fuel cell and found similar results for oxidation peak [59]. The highest current densities for BH_4^- oxidation were obtained on PtAu/CNT-G catalyst (a_2') suggesting an enhanced catalytic activity than Au/CNT-G (a_2) and Pt/CNT-G (a_2'') catalysts due to the synergistic interaction between Pt and Au particles on CNT-G support. During the reverse sweep, an anodic peaks (c_2, c_2' and c_2'') corresponds the adsorbed BH_3OH^-, which might be seen as an intermediate during the oxidation of BH_4^- obtained during the direct sweep. Similar peaks were obtained from Liu et al. [32].

RDE technique was applied to examine the BOR kinetics of the catalysts. Koutecky-Levich equation was used to calculate the number of exchanged electrons (n) involved in borohydride oxidation (Equation (8)) [60].

$$\frac{1}{j}=\frac{1}{j_K}+\frac{1}{j_L}=\frac{1}{j_K}+\frac{1}{0.62nFD^{\frac{2}{3}}C\nu^{-\frac{1}{6}}\omega^{\frac{1}{2}}}=\frac{1}{j_K}+\frac{1}{B\omega^{\frac{1}{2}}} \quad (8)$$

where j is the measured current density, j_L is the diffusion convection limit current density and j_k is the kinetic-controlled current density, n is the transfer electron number of BOR, F is the Faraday constant (96,485 C mol^{-1}), D is the electrolyte solution diffusion coefficient (1.35×10^{-5} cm^2 s^{-1}) [61], C is the volumetric concentration of the electrolyte solution (mol L^{-1}), ν is the kinetic viscosity of the solution (0.0114 cm^2 s^{-1}) [62], ω is the angular velocity of the RDE rotation.

Fig. 7 illustrates the parallelism of Koutecky-Levich plots for different potentials. As seen from Fig. 7 the onset for BH_4^- oxidation is at about −0.65 V vs. Ag/AgCl, and the currents increase with the increase of rotation rate for Au/CNT-G catalyst. Similar results are found Yi et al. for Au/C catalyst [63]. The apparent number of electrons involved in BH_4 electrooxidation at the Au/C, PtAu/CNT-G and Pt/CNT-G electrodes were calculated as $n_{Au/C} = 8$, $n_{PtAu/CNT-G} = 7$ and $n_{Pt/CNT-G} = 7.4$ respectively.

3.3. $NaBH_4/H_2O_2$ fuel cell tests

3.3.1. Effect of temperature

Operating temperature is an important parameter to avoid performance losses in fuel cell. However, it is important to determine the optimum cell working temperature, since increasing the operating temperature greatly increases the hydrolysis of $NaBH_4$ and decomposition of H_2O_2. To investigate the effect of the catalysts on $NaBH_4/H_2O_2$ fuel cell performance, membrane electrode assemblies using Nafion 115 membrane solution containing 2 M NaOH at 25 °C.

Fig. 8 presents the $NaBH_4/H_2O_2$ polarization curves and the corresponding power density curves by employing the PtAu/CNT-G as the anode catalyst with 2 M $NaBH_4$ in 6 M NaOH as anode side reactant and 2 M H_2O_2 in 1 M HCl as cathode side oxidant at 25–50 °C working temperatures. For comparison, the temperature effect on the performance of Au/CNT-G and Pt/CNT-G catalysts were also examined.

Table 2 shows the comparison of the OCV and the peak power density of the prepared catalyst. The OCV values of the $NaBH_4/H_2O_2$ fuel cell using PtAu/CNT-G as catalyst were observed 1.65, 1.7 and 1.75 V at 25, 40 and 50 °C, respectively. The highest OCV values were obtained for PtAu/CNT-G catalyst at all temperature. The cell performance was improved with increasing working temperature as expected. The highest power density was observed for PtAu/CNT-G based MEA as 103, 118 and 139 mW/cm^2, at 25, 40 and 50 °C, respectively. The maximum power density was observed for

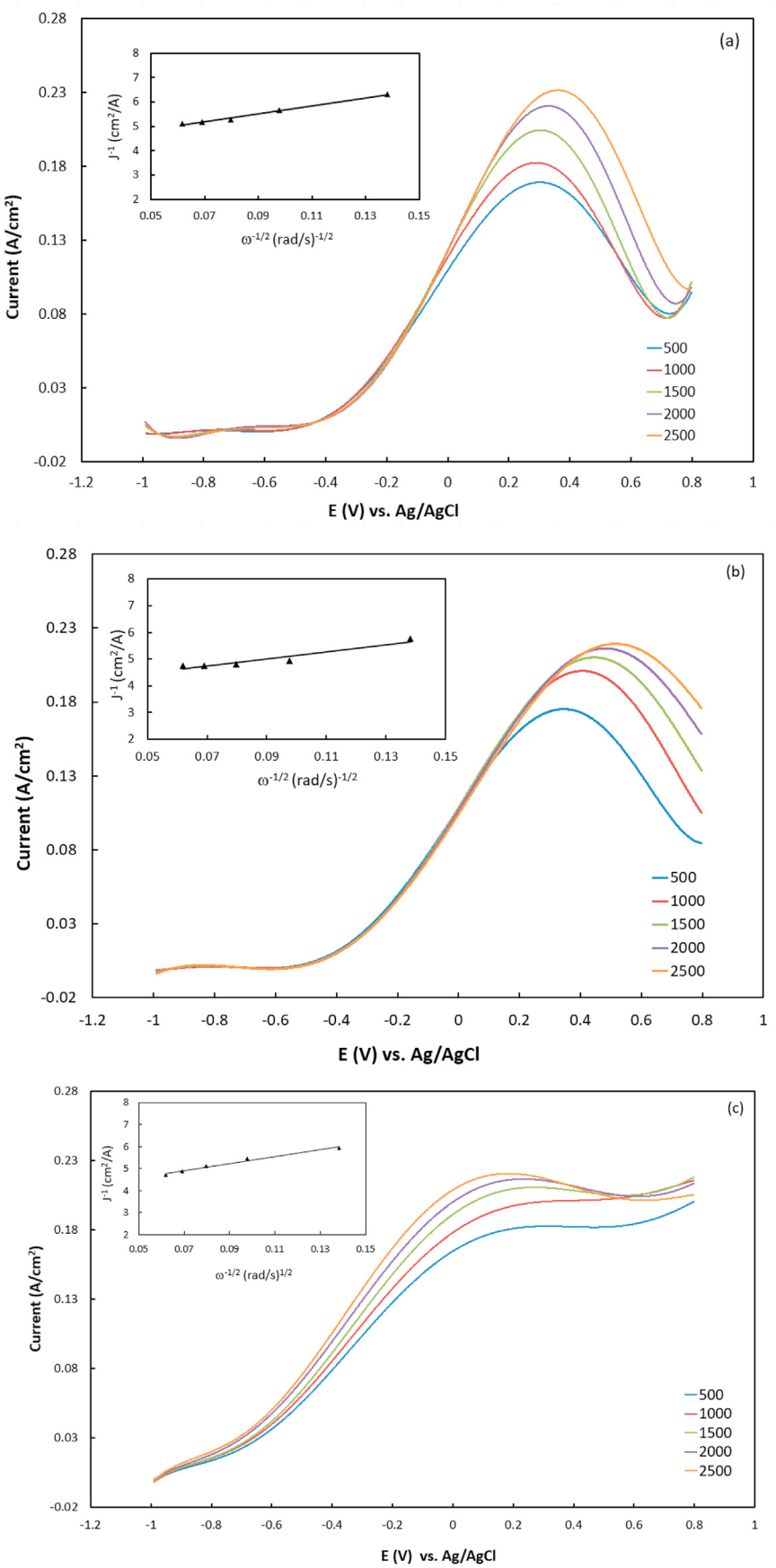

Fig. 7. RDE voltammogram curves of (a) PtAu/CNT-G, (b) Au/CNT-G and c) Pt/CNT-G with different rotation rates in 0.12 M NaBH4 + 2 M NaOH at the scan rate of 20 mV/s.

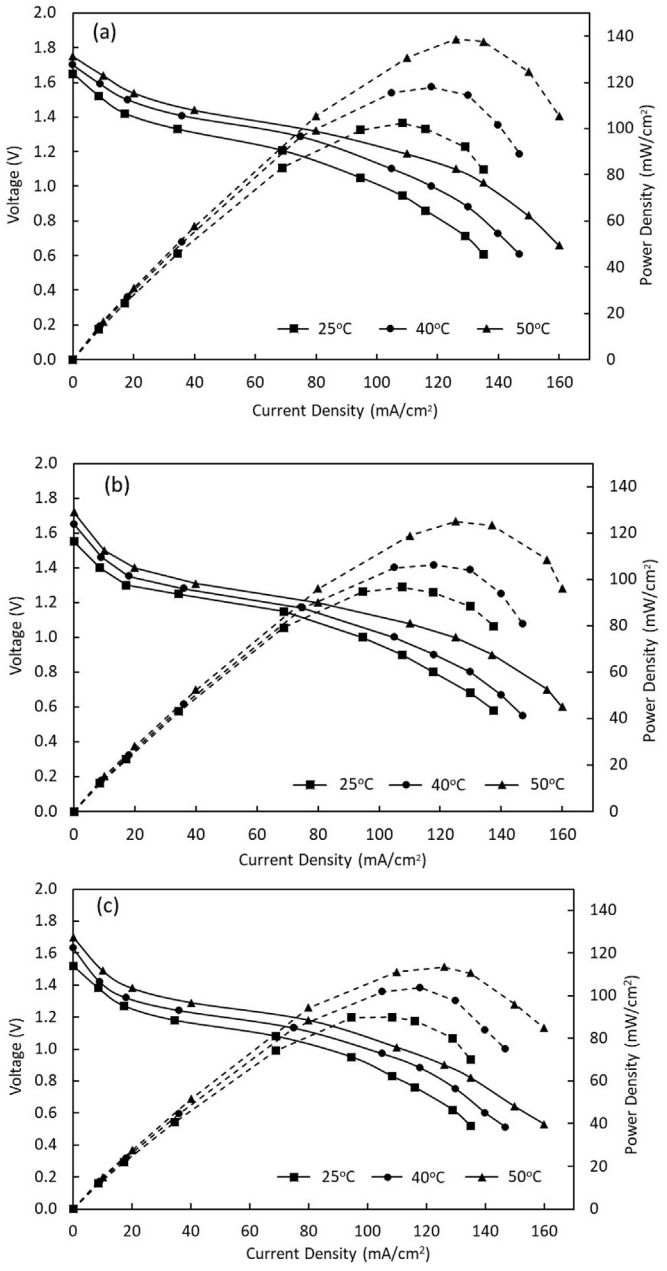

Fig. 8. Cell polarization and power density curves of a) PtAu/CNT-G b) Au/CNT-G and c) Pt/CNT-G catalysts temperatures ranging from 25 to 50 °C (Anolyte: 2 M $NaBH_4$ + 6 M NaOH; Catholyte: 2 M H_2O_2 + 1 M HCl).

Table 2
Comparison of the OCV and peak power density of the prepared catalyst.

Catalyst	OCV (V)			Peak power density (mW/cm^2)		
	25 (°C)	40 (°C)	50 (°C)	25 (°C)	40 (°C)	50 (°C)
PtAu/CNT-G	1.65	1.70	1.75	103	118	139
Au/CNT-G	1.55	1.65	1.72	97	106	125
Pt/CNT-G	1.52	1.64	1.70	90	104	113

Au/CNT-G based MEA as 97, 106 and 125 mW/cm^2, at 25, 40 and 50 °C, respectively. Under the same fuel cell working conditions, the highest performance for Pt/CNT-G catalyst was achieved as 90, 104 and 113 mW/cm^2, at 25, 40 and 50 °C, respectively. Although PtAu/CNT-G catalyst has lower ECSA than Pt/CNT-G catalyst, it was shown the most efficient catalyst among the other prepared catalysts for $NaBH_4/H_2O_2$ fuel cell. The enhanced fuel cell performance could be attributed to synergistic effects between the PtAu bimetallic catalyst and the CNT-G support material [46]. It is observed that the performance of all catalyst was increased by increasing the temperature for all catalyst. The increase in $NaBH_4/H_2O_2$ performance at higher temperatures can be attributed to the enhanced kinetics of both the anodic and cathodic reactions [64–66].

3.3.2. *Effect of $NaBH_4$ concentration*

The effect of $NaBH_4$ concentration on $NaBH_4/H_2O_2$ fuel cell performance of the PtAu/CNT-G catalyst at 50 °C is shown in Fig. 9. When the $NaBH_4$ concentration was 0.5, 1, 2 and 3 M, the highest power density was 107, 116, 139 and 125 mW/cm^2, respectively. Borohydride oxidation rate increases with increasing $NaBH_4$ concentration and the best fuel cell performance was achieved with 2 M $NaBH_4$. However, excessive concentration decreases performance by increasing $NaBH_4$ cross over and increasing borohydride hydrolysis [64].

3.3.3. *Effect of H_2O_2 concentration*

To study the influence of H_2O_2 concentration on the $NaBH_4/H_2O_2$ performance, the working temperature was kept at 50 °C and the current-voltage and current-power polarization curves of a $NaBH_4/H_2O_2$ under different H_2O_2 concentration were investigated. Fig. 10 shows the effect of H_2O_2 concentration on $NaBH_4/H_2O_2$ fuel cell performance at 50 °C.

As shown in Fig. 10, the increase in maximum power density was determined by increasing the H_2O_2 concentration from 0.5 to 2 M. However, cell performance decreased as H_2O_2 concentration increased to 3 M. With increasing H_2O_2 concentration, cathode potential increased according to Nernst equation. However, as the H_2O_2 concentration increases too much, the crossover of H_2O_2 from the membrane increases and this decreases the voltage. When the H_2O_2 concentration was 0.5, 1, 2 and 3 M, the highest power density was 93, 111, 139 and 117 mW/cm^2, respectively. The noble-metal-type catalysts as Pt generally tends to decompose peroxide very quickly, although they do provide excellent fuel cell performance [67]. In this study, commercial Pt/C catalysts were used on the cathode side and possible H_2O_2 degradation increased due to the increase in H_2O_2 concentration.

Fig. 11 illustrates the short term stability of $NaBH_4/H_2O_2$ fuel cell performance of the PtAu/CNT-G catalyst at 50 °C. Stability of the $NaBH_4/H_2O_2$ fuel cell was tested by monitoring the cell voltage change vs. time at a constant current density of 135 mA/cm^2. The cell using PtAu/CNT-G catalyst maintained 98% of its voltage after 10 h short term stability test. According to the results of experiments, PtAu/CNT-G catalyst can be a potential candidate for enhanced $NaBH_4/H_2O_2$ fuel cell performance.

Peak power densities of the different catalysts used in direct $NaBH_4/H_2O_2$ fuel cell in the literature are listed in Table 3 for comparison. Compared to the literature, both PtAu/CNT-G and Au/CNT-G catalysts gave higher performance. When Au/CNT-G catalyst and PtAu/CNT-G catalyst was compared, it was seen that PtAu/CNT-G shows higher performance. The observed improvement in $NaBH_4/H_2O_2$ fuel cell in the presence of the PtAu/CNT-G catalyst was mainly due to the increase in the number of active sites by increasing surface area with CNT-G support and the metal interaction in the bimetallic catalysts. Therefore, it could be concluded from the comparison that the synthesized PtAu/CNT-G is efficient catalyst for direct $NaBH_4/H_2O_2$ fuel cell application.

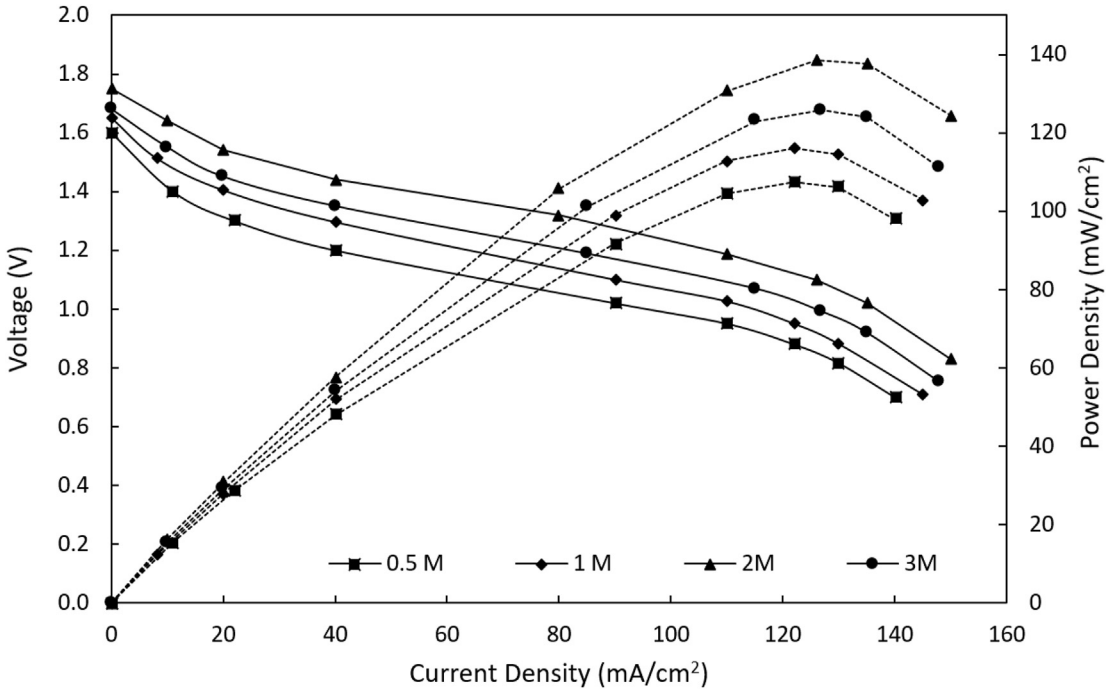

Fig. 9. Effect of the $NaBH_4$ concentration on $NaBH_4/H_2O_2$ fuel cell performances of the PtAu/CNT-G catalyst at 50 °C (Catholyte: 2 M H_2O_2 + 1 M HCl).

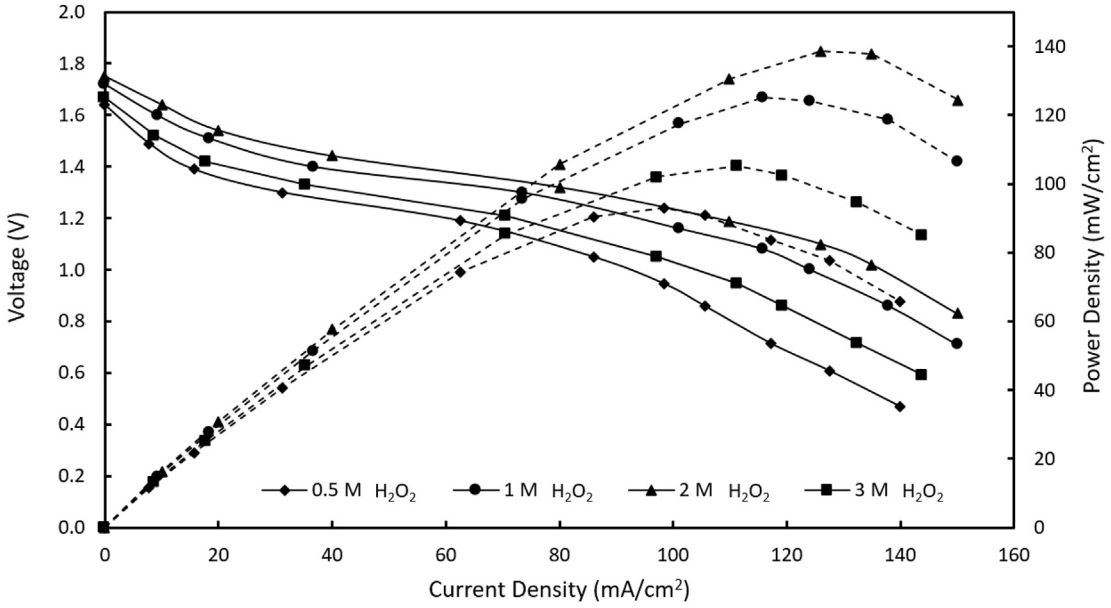

Fig. 10. Effect of the H_2O_2 concentration on $NaBH_4/H_2O_2$ fuel cell performances of the PtAu/CNT-G catalyst at 50 °C (Anolyte: 2 M $NaBH_4$ + 6 M NaOH).

4. Conclusion

In this study, CNT-G hybrid material supported catalysts were prepared as an efficient anode catalyst for $NaBH_4/H_2O_2$ fuel cell. The chemical reduction synthesis method was applied to prepare the PtAu/CNT-G, Au/CNT-G and Pt/CNT-G catalysts. The structure of catalysts was characterized by TGA, XRD, ICP-OES and TEM analysis. The incorporation of CNT into G decreases the sticking of the graphene sheets due to π−π interactions and the higher loading of dispersed Pt nanoparticles, resulting in the enhanced electrocatalytic activity of the prepared electrocatalysts. TEM images proved that metal particles were uniformly dispersed in the mixed carbon substrates with slight agglomeration. It was found that the particle size of the PtAu/CNT-G was ~7 nm with good particle dispersion. In addition, the electrocatalytic activity of the catalysts was investigated by CV analysis. It has been found by CV and RDE analyses that the Au/CNT-G and PtAu/CNT-G catalysts show higher electrocatalytic activity for the direct BH_4 electrooxidation. $NaBH_4/H_2O_2$ fuel cell performances under different operation conditions were studied including operation temperature, $NaBH_4$ concentration, and H_2O_2 concentration. According to the $NaBH_4/H_2O_2$ fuel cell performance experiments, highest maximum power density of

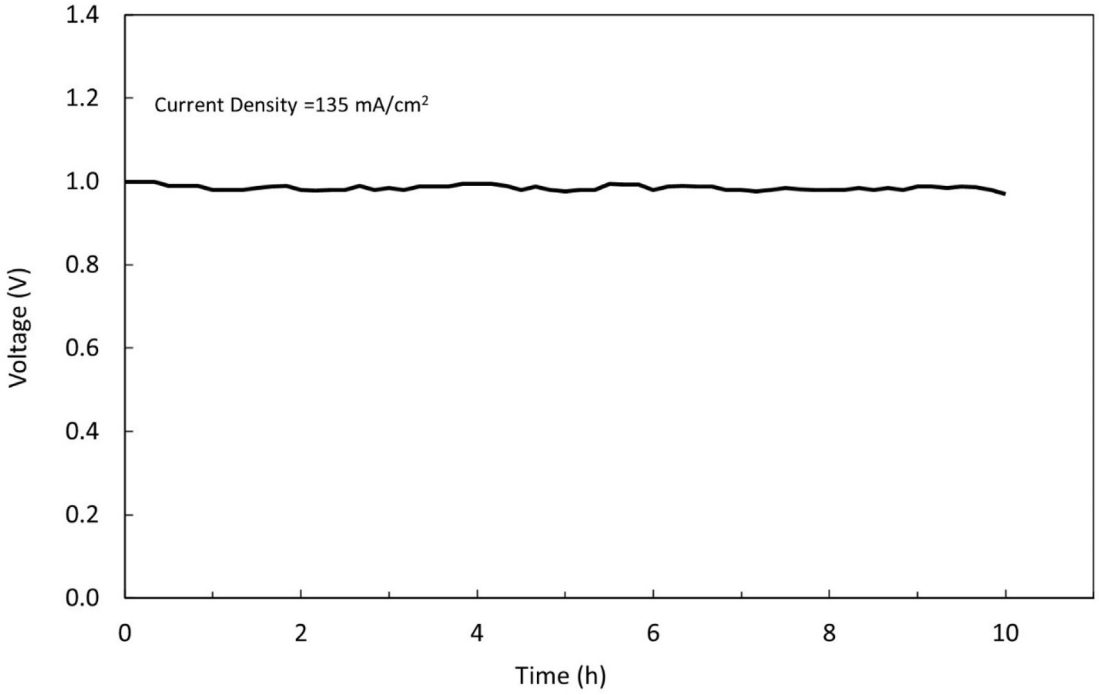

Fig. 11. Short term stability test of $NaBH_4/H_2O_2$ fuel cell performances of the PtAu/CNT-G catalyst at 50 °C (Anolyte: 2 M $NaBH_4$ + 6 M NaOH).

Table 3
Comparison of the $NaBH_4/H_2O_2$ fuel cell anode catalysts.

Anode catalyst	Cathode catalyst	Membrane	Temperature (°C)	Peak power density (mW/cm^2)	Reference
Pt/C	Pt/C	Nafion 117	25	35	[68]
NiPt/C	Pt/C	Nafion 117	60	133.4	[69]
$Pt_{67}Sn_{33}/C$	Pt/C	Nafion 117	25	91.5	[70]
$Pt_{67}Co_{33}/C$	Pt/C	Nafion 117	25	79.7	[70]
$Pt_{50}Cu_{50}/C$	Pt/C	Nafion 117	25	79.9	[71]
Au/C	Pt/C	Nafion 117	20	34	[72]
Au/C	Pt/C	Nafion 117	60	85	[56]
Au	Pt/C	Nafion 115	27	33	[73]
$Au_{67}Cu_{33}/C$	Au/C	Nafion 117	20	46	[74]
AuZn/C	Au/C	Nafion 117	20	40	[75]
PtAu/C	Pt/C	Nafion 115	65	161	[76]
PtAu/C	Pt/C	Nafion 115	40	112	[76]
$Pt_{50}Au_{50}$/CNT-G	Pt/C	Nafion 115	50	139	This study
Au/CNT-G	Pt/C	Nafion 115	50	125	This study

the PtAu/CNT-G catalyst was observed as 139 mWcm $^{-2}$ for 2 M $NaBH_4$ in 6 M NaOH anolyte and 2 M H_2O_2 in 1 M HCl catholyte at 50 °C. The results of fuel cell tests indicate that PtAu/CNT-G catalyst is a potential candidate for enhanced $NaBH_4/H_2O_2$ fuel cell performance.

CRediT authorship contribution statement

Arife Uzundurukan: Investigation. **Elif Seda Akça:** Investigation. **Yağmur Budak:** Investigation. **Yılser Devrim:** Conceptualization, Methodology, Investigation, Writing - original draft.

Declaration of competing interest

The authors declare that they have no known competing financial interests or personal relationships that could have appeared to influence the work reported in this paper.

Acknowledgements

The authors gratefully acknowledge funding from the Atılım University (Grant Number: ATU-LAP-1819-01). The authors would like to thank to TEKSIS Company (Turkey) for providing technical support on manufacturing of GDE's by the ultrasonic coating system.

References

[1] F.A. Coowar, G. Vitins, G.O. Mepsted, S.C. Waring, J.A. Horsfall, Electrochemical oxidation of borohydride at nano-gold-based electrodes: application in direct borohydride fuel cells, J. Power Sources 175 (2008) 317–324, https://doi.org/10.1016/j.jpowsour.2007.09.063.
[2] G.H. Miley, N. Luo, J. Mather, R. Burton, G. Hawkins, L. Gu, et al., Direct NaBH4/H2O2 fuel cells, J. Power Sources 165 (2007) 509–516, https://doi.org/10.1016/j.jpowsour.2006.10.062.
[3] T.H. Oh, B. Jang, S. Kwon, Estimating the energy density of direct borohydride-hydrogen peroxide fuel cell systems for air-independent propulsion applications, Energy 90 (2015) 980–986, https://doi.org/10.1016/j.energy.2015.08.002.

[4] N. Luo, G.H. Miley, K.J. Kim, R. Burton, X. Huang, NaBH4/H2O2 fuel cells for air independent power systems, J. Power Sources 185 (2008) 685–690, https://doi.org/10.1016/j.jpowsour.2008.08.090.
[5] P. Folly, P. Mäder, Propellant chemistry, Chimia 58 (2004) 374–382, https://doi.org/10.2533/000942904777677713.
[6] J. Ma, Y. Sahai, R.G. Buchheit, Direct borohydride fuel cell using Ni-based composite anodes, J. Power Sources 195 (2010) 4709–4713, https://doi.org/10.1016/j.jpowsour.2010.02.034.
[7] S.R. Choudhury, M.B. Deshmukh, R. Rengaswamy, A two-dimensional steady-state model for phosphoric acid fuel cells (PAFC), J. Power Sources 112 (2002) 137–152, https://doi.org/10.1016/S0378-7753(02)00369-5.
[8] T.H. Oh, Design specifications of direct borohydride–hydrogen peroxide fuel cell system for space missions, Aero. Sci. Technol. 58 (2016) 511–517, https://doi.org/10.1016/j.ast.2016.09.012.
[9] R.O. Stroman, G.S. Jackson, Modeling the performance of an ideal NaBH4-H2O 2 direct borohydride fuel cell, J. Power Sources 247 (2014) 756–769, https://doi.org/10.1016/j.jpowsour.2013.08.100.
[10] M. Abdolmaleki, M.G. Hosseini, A development in direct borohydride/hydrogen peroxide fuel cell using nanostructured Ni-Pt/C anode, Fuel Cell. 17 (2017) 321–327, https://doi.org/10.1002/fuce.201600134.
[11] R. Valiollahi, R. Ojani, Pt hollow nanospheres/graphene electrocatalytic ability toward sodium borohydride oxidation: a study of morphology effect on electrocatalytic activity, J. Appl. Electrochem. 47 (2017) 205–212, https://doi.org/10.1007/s10800-016-1009-2.
[12] K. Cheng, J. Jiang, S. Kong, Y. Gao, K. Ye, G. Wang, et al., Pd nanoparticles support on rGO-C@TiC coaxial nanowires as a novel 3D electrode for NaBH4 electrooxidation, Int. J. Hydrogen Energy 42 (2017) 2943–2951, https://doi.org/10.1016/j.ijhydene.2016.11.156.
[13] D. Zhang, G. Wang, Y. Yuan, Y. Li, S. Jiang, Y. Wang, et al., Three-dimensional functionalized graphene networks modified Ni foam based gold electrode for sodium borohydride electrooxidation, Int. J. Hydrogen Energy 41 (2016) 11593–11598, https://doi.org/10.1016/j.ijhydene.2016.04.106.
[14] L. Tamašauskaitė-Tamašiūnaitė, A. Balčiūnaitė, R. Čekavičiūtė, A. Selskis, Investigation of titanium supported nanostructured Au-Ni and Pt-Ni thin layers as electrocatalysts for DBFC, J. Electrochem. Soc. 159 (2012) B611–B618, https://doi.org/10.1149/2.026206jes.
[15] L.C. Nagle, J.F. Rohan, Nanoporous gold anode catalyst for direct borohydride fuel cell, in: EFC 2009 - Piero Lunghi Conf. Proc. 3rd Eur. Fuel Cell Technol. Appl. Conf., 2009, pp. 321–322.
[16] M. Chatenet, F. Micoud, I. Roche, E. Chainet, Kinetics of sodium borohydride direct oxidation and oxygen reduction in sodium hydroxide electrolyte. Part I. BH4- electro-oxidation on Au and Ag catalysts, Electrochim. Acta 51 (2006) 5459–5467, https://doi.org/10.1016/j.electacta.2006.02.015.
[17] B.H. Liu, Z.P. Li, S. Suda, Solid sodium borohydride as a hydrogen source for fuel cells, J. Alloys Compd. 468 (2009) 493–498, https://doi.org/10.1016/j.jallcom.2008.01.023.
[18] X. Geng, H. Zhang, W. Ye, Y. Ma, H. Zhong, Ni-Pt/C as anode electrocatalyst for a direct borohydride fuel cell, J. Power Sources 185 (2008) 627–632, https://doi.org/10.1016/j.jpowsour.2008.09.010.
[19] M.H. Atwan, D.O. Northwood, E.L. Gyenge, Evaluation of colloidal Os and Os-alloys (Os-Sn, Os-Mo and Os-V) for electrocatalysis of methanol and boro-hydride oxidation, Int. J. Hydrogen Energy 30 (2005) 1323–1331, https://doi.org/10.1016/j.ijhydene.2005.04.010.
[20] T.H. Oh, B. Jang, S. Kwon, Electrocatalysts supported on multiwalled carbon nanotubes for direct borohydride-hydrogen peroxide fuel cell, Int. J. Hydrogen Energy 39 (2014) 6977–6986, https://doi.org/10.1016/j.ijhydene.2014.02.117.
[21] A. Tegou, S. Papadimitriou, I. Mintsouli, S. Armyanov, E. Valova, G. Kokkinidis, et al., Rotating disc electrode studies of borohydride oxidation at Pt and bimetallic Pt-Ni and Pt-Co electrodes, Catal. Today 170 (2011) 126–133, https://doi.org/10.1016/j.cattod.2011.01.003.
[22] X. Guo, D.J. Guo, X.P. Qiu, L.Q. Chen, W.T. Zhu, A simple one-step preparation of high utilization AuPt nanoparticles supported on MWCNTs for methanol oxidation in alkaline medium, Electrochem. Commun. 10 (2008) 1748–1751, https://doi.org/10.1016/j.elecom.2008.09.005.
[23] D. Cameron, R. Holliday, D. Thompson, Gold's future role in fuel cell systems, J. Power Sources (2003), https://doi.org/10.1016/S0378-7753(03)00074-0.
[24] J. Luo, P.N. Njoki, Y. Lin, D. Mott, L. Wang, C.J. Zhong, Characterization of carbon-supported AuPt nanoparticles for electrocatalytic methanol oxidation reaction, Langmuir 22 (2006) 2892–2898, https://doi.org/10.1021/la0529557.
[25] H. You, F. Zhang, Z. Liu, J. Fang, Free-standing Pt-Au hollow nanourchins with enhanced activity and stability for catalytic methanol oxidation, ACS Catal. 4 (2014) 2829–2835, https://doi.org/10.1021/cs500390s.
[26] H. Zhang, N. Toshima, Synthesis of Au/Pt bimetallic nanoparticles with a Pt-rich shell and their high catalytic activities for aerobic glucose oxidation, J. Colloid Interface Sci. 394 (2013) 166–176, https://doi.org/10.1016/j.jcis.2012.11.059.
[27] S. Litster, G. McLean, PEM fuel cell electrodes, J. Power Sources 130 (2004) 61–76, https://doi.org/10.1016/j.jpowsour.2003.12.055.
[28] Z. Chen, D. Higgins, A. Yu, L. Zhang, J. Zhang, A review on non-precious metal electrocatalysts for PEM fuel cells, Energy Environ. Sci. 4 (2011) 3167–3192, https://doi.org/10.1039/c0ee00558d.
[29] S. Samad, K.S. Loh, W.Y. Wong, T.K. Lee, J. Sunarso, S.T. Chong, et al., Carbon and non-carbon support materials for platinum-based catalysts in fuel cells, Int. J. Hydrogen Energy 43 (2018) 7823–7854, https://doi.org/10.1016/j.ijhydene.2018.02.154.
[30] E. Antolini, Carbon supports for low-temperature fuel cell catalysts, Appl. Catal. B Environ. 88 (2009) 1–24, https://doi.org/10.1016/j.apcatb.2008.09.030.
[31] M. Liu, C. Zhang, W. Chen, Novel Nanomaterials as Electrocatalysts for Fuel Cells, Elsevier Inc., 2018, https://doi.org/10.1016/B978-0-12-813731-4.00006-0.
[32] X. Liu, L. Yi, X. Wang, J. Su, Y. Song, J. Liu, Graphene supported platinum nanoparticles as anode electrocatalyst for direct borohydride fuel cell, Int. J. Hydrogen Energy 37 (2012) 17984–17991, https://doi.org/10.1016/j.ijhydene.2012.09.136.
[33] S.A. Grigoriev, V.N. Fateev, A.S. Pushkarev, I.V. Pushkareva, N.A. Ivanova, V.N. Kalinichenko, et al., Reduced graphene oxide and its modifications as catalyst supports and catalyst layer modifiers for PEMFC, Materials 11 (2018), https://doi.org/10.3390/ma11081405.
[34] A. Bayrakçeken Yurtcan, E. Daş, Chemically synthesized reduced graphene oxide-carbon black based hybrid catalysts for PEM fuel cells, Int. J. Hydrogen Energy 43 (2018) 18691–18701, https://doi.org/10.1016/j.ijhydene.2018.06.186.
[35] W. Zhang, J. Chen, G.F. Swiegers, Z.F. Ma, G.G. Wallace, Microwave-assisted synthesis of Pt/CNT nanocomposite electrocatalysts for PEM fuel cells, Nanoscale 2 (2010) 282–286, https://doi.org/10.1039/b9nr00140a.
[36] H. El-Deeb, M. Bron, Microwave-assisted polyol synthesis of PtCu/carbon nanotube catalysts for electrocatalytic oxygen reduction, J. Power Sources 275 (2015) 893–900, https://doi.org/10.1016/j.jpowsour.2014.11.060.
[37] S. Takenaka, H. Matsumori, H. Matsune, E. Tanabe, M. Kishida, High durability of carbon nanotube-supported Pt electrocatalysts covered with silica layers for the cathode in a PEMFC, J. Electrochem. Soc. 155 (2008) B929, https://doi.org/10.1149/1.2952665.
[38] Y. Devrim, E.D. Arıca, Multi-walled carbon nanotubes decorated by platinum catalyst for high temperature PEM fuel cell, Int. J. Hydrogen Energy 44 (2019) 18951–18966, https://doi.org/10.1016/j.ijhydene.2019.01.051.
[39] Ş.B. Barım, A. Bayrakçeken, S.E. Bozbağ, L. Zhang, R. Kızılel, M. Aindow, et al., Control of average particle size of carbon aerogel supported platinum nanoparticles by supercritical deposition, Microporous Mesoporous Mater. 245 (2017) 94–103, https://doi.org/10.1016/j.micromeso.2017.01.037.
[40] S. Sharma, B.G. Pollet, Support materials for PEMFC and DMFC electrocatalysts - a review, J. Power Sources 208 (2012) 96–119, https://doi.org/10.1016/j.jpowsour.2012.02.011.
[41] V. Singh, D. Joung, L. Zhai, S. Das, S.I. Khondaker, S. Seal, Graphene based materials: past, present and future, Prog. Mater. Sci. 56 (2011) 1178–1271, https://doi.org/10.1016/j.pmatsci.2011.03.003.
[42] S.H. Hur, J.N. Park, Graphene and its application in fuel cell catalysis: a review, Asia Pac. J. Chem. Eng. 8 (2013) 218–233, https://doi.org/10.1002/apj.1676.
[43] N.M. Julkapli, S. Bagheri, Graphene supported heterogeneous catalysts: an overview, Int. J. Hydrogen Energy 40 (2015) 948–979, https://doi.org/10.1016/j.ijhydene.2014.10.129.
[44] A. Bharti, G. Cheruvally, Influence of various carbon nano-forms as supports for Pt catalyst on proton exchange membrane fuel cell performance, J. Power Sources 360 (2017) 196–205, https://doi.org/10.1016/j.jpowsour.2017.05.117.
[45] A. Uzundurukan, Y. Devrim, Carbon nanotube-graphene hybrid supported platinum as an effective catalyst for hydrogen generation from hydrolysis of ammonia borane, Int. J. Hydrogen Energy 44 (2019) 26773–26782, https://doi.org/10.1016/j.ijhydene.2019.08.153.
[46] Alpaydin Gu, Y. Devrim, C.O. Colpan, Performance of an HT-PEMFC having a catalyst with graphene and multiwalled carbon nanotube support, Int. J. Energy Res. 43 (2019) 3578–3589, https://doi.org/10.1002/er.4504.
[47] S.G. da Silva, J.C.M. Silva, G.S. Buzzo, A.O. Neto, MôHMT. Assumpção, Use of ptau/c electrocatalysts toward formate oxidation: electrochemical and fuel cell considerations, Mater Renew Sustain Energy 5 (2016), https://doi.org/10.1007/s40243-016-0079-8.
[48] Y. Devrim, E.D. Arıca, Investigation of the effect of graphitized carbon nanotube catalyst support for high temperature PEM fuel cells, Int. J. Hydrogen Energy 45 (2020) 3609–3617, https://doi.org/10.1016/j.ijhydene.2019.01.111.
[49] Y. Devrim, Preparation and testing of Nafion/titanium dioxide nanocomposite membrane electrode assembly by ultrasonic coating technique, J. Appl. Polym. Sci. 131 (2014), https://doi.org/10.1002/app.40541.
[50] Y. Devrim, E.D. Arıca, A. Albostan, Graphene based catalyst supports for high temperature PEM fuel cell application, Int. J. Hydrogen Energy 43 (2018) 11820–11829, https://doi.org/10.1016/j.ijhydene.2018.03.047.
[51] A. Primo, I. Esteve-Adell, S.N. Coman, N. Candu, V.I. Parvulescu, H. Garcia, One-step pyrolysis preparation of 1.1.1 oriented gold nanoplatelets supported on graphene and six orders of magnitude enhancement of the resulting catalytic activity, Angew. Chem. Int. Ed. 55 (2016) 607–612, https://doi.org/10.1002/anie.201508908.
[52] P.B. Kowalczuk, J. Drzymala, Physical meaning of the Sauter mean diameter of spherical particulate matter, Part. Sci. Technol. 34 (2016) 645–647, https://doi.org/10.1080/02726351.2015.1099582.
[53] J.B. Xu, T.S. Zhao, W.W. Yang, S.Y. Shen, Effect of surface composition of Pt-Au alloy cathode catalyst on the performance of direct methanol fuel cells, Int. J. Hydrogen Energy 35 (2010) 8699–8706, https://doi.org/10.1016/j.ijhydene.2010.05.008.
[54] Y. Devrim, E.D. Arıca, Multi-walled carbon nanotubes decorated by platinum catalyst for high temperature PEM fuel cell, Int. J. Hydrogen Energy 44 (2019) 18951–18966, https://doi.org/10.1016/j.ijhydene.2019.01.051.

[55] L. Yi, Y. Meng, S. Yang, J. Fei, Y. Ding, X. Wang, et al., N-Doped carbon-supported Au-modified NiFe alloy nanoparticle composite catalysts for BH4−electrooxidation, New J. Chem. (2020), https://doi.org/10.1039/d0nj00557f.
[56] F. Pei, Y. Wang, X. Wang, P.Y. He, L. Liu, Y. Xu, et al., Preparation and performance of highly efficient Au nanoparticles electrocatalyst for the direct borohydride fuel cell, Fuel Cell. 11 (2011) 595–602, https://doi.org/10.1002/fuce.200900207.
[57] M.V. Mirkin, Borohydride oxidation at a gold electrode, J. Electrochem. Soc. 139 (1992) 2212, https://doi.org/10.1149/1.2221204.
[58] M.H. Atwan, C.L.B. Macdonald, D.O. Northwood, E.L. Gyenge, Colloidal Au and Au-alloy catalysts for direct borohydride fuel cells: electrocatalysis and fuel cell performance, J. Power Sources 158 (2006) 36–44, https://doi.org/10.1016/j.jpowsour.2005.09.054.
[59] E. Gyenge, Electrooxidation of borohydride on platinum and gold electrodes: implications for direct borohydride fuel cells, Electrochim. Acta 49 (2004) 965–978, https://doi.org/10.1016/j.electacta.2003.10.008.
[60] D.A. Finkelstein, N. Da Mota, J.L. Cohen, H.D. Abruña, Rotating disk electrode (RDE) investigation of BH4- and BH3OH-electro-oxidation at Pt and Au: implications for BH 4- fuel cells, J. Phys. Chem. C (2009), https://doi.org/10.1021/jp900933c.
[61] K. Wang, J. Lu, L. Zhuang, Direct determination of diffusion coefficient for borohydride anions in alkaline solutions using chronoamperometry with spherical Au electrodes, J. Electroanal. Chem. (2005), https://doi.org/10.1016/j.jelechem.2005.08.009.
[62] C. Ponce de León, F.C. Walsh, C.J. Patrissi, M.G. Medeiros, R.R. Bessette, R.W. Reeve, et al., A direct borohydride-peroxide fuel cell using a Pd/Ir alloy coated microfibrous carbon cathode, Electrochem. Commun. (2008), https://doi.org/10.1016/j.elecom.2008.08.006.
[63] L. Yi, W. Wei, C. Zhao, L. Tian, J. Liu, X. Wang, Enhanced activity of Au-Fe/C anodic electrocatalyst for direct borohydride-hydrogen peroxide fuel cell, J. Power Sources (2015), https://doi.org/10.1016/j.jpowsour.2015.03.118.
[64] W. Haijun, W. Cheng, L. Zhixiang, M. Zongqiang, Influence of operation conditions on direct NaBH4/H2O2 fuel cell performance, Int. J. Hydrogen Energy 35 (2010) 2648–2651, https://doi.org/10.1016/j.ijhydene.2009.04.020.
[65] N.A. Choudhury, R.K. Raman, S. Sampath, A.K. Shukla, An alkaline direct borohydride fuel cell with hydrogen peroxide as oxidant, J. Power Sources 143 (2005) 1–8, https://doi.org/10.1016/j.jpowsour.2004.08.059.
[66] X. Yan, F. Meng, Y. Xie, J. Liu, Y. Ding, Direct N2H4/H2O2 fuel cells powered by nanoporous gold leaves, Sci. Rep. 2 (2012), https://doi.org/10.1038/srep00941.
[67] G.H. Miley, N. Luo, J. Mather, R. Burton, G. Hawkins, L. Gu, et al., Direct NaBH4/H2O2 fuel cells, J. Power Sources (2007), https://doi.org/10.1016/j.jpowsour.2006.10.062.
[68] L. Yi, B. Yu, W. Yi, Y. Zhou, R. Ding, X. Wang, Carbon-supported bimetallic platinum-iron nanocatalysts: application in direct borohydride/hydrogen peroxide fuel cell, ACS Sustain. Chem. Eng. 6 (2018) 8142–8149, https://doi.org/10.1021/acssuschemeng.7b04438.
[69] M.G. Hosseini, R. Mahmoodi, Preparation method of Ni@Pt/C nanocatalyst affects the performance of direct borohydride-hydrogen peroxide fuel cell: improved power density and increased catalytic oxidation of borohydride, J. Colloid Interface Sci. 500 (2017) 264–275, https://doi.org/10.1016/j.jcis.2017.04.016.
[70] L. Yi, L. Liu, X. Wang, X. Liu, W. Yi, X. Wang, Carbon supported Pt-Sn nanoparticles as anode catalyst for direct borohydride-hydrogen peroxide fuel cell: electrocatalysis and fuel cell performance, J. Power Sources 224 (2013) 6–12, https://doi.org/10.1016/j.jpowsour.2012.09.082.
[71] L. Yi, B. Hu, Y. Song, X. Wang, G. Zou, W. Yi, Studies of electrochemical performance of carbon supported Pt-Cu nanoparticles as anode catalysts for direct borohydride-hydrogen peroxide fuel cell, J. Power Sources 196 (2011) 9924–9930, https://doi.org/10.1016/j.jpowsour.2011.08.063.
[72] C.P. de León, F.C. Walsh, A. Rose, J.B. Lakeman, D.J. Browning, R.W. Reeve, A direct borohydride-Acid peroxide fuel cell, J. Power Sources 164 (2007) 441–448, https://doi.org/10.1016/j.jpowsour.2006.10.069.
[73] R.W. Reeve, A sodium borohydride - hydrogen peroxide fuel cell employing a bipolar membrane electrolyte, ECS Trans (2012) 117–129, https://doi.org/10.1149/1.4705487.
[74] N.A. Choudhury, J. Ma, Y. Sahai, R.G. Buchheit, High performance polymer chemical hydrogel-based electrode binder materials for direct borohydride fuel cells, J. Power Sources 196 (2011) 5817–5822, https://doi.org/10.1016/j.jpowsour.2011.03.004.
[75] P. He, X. Wang, P. Fu, H. Wang, L. Yi, The studies of performance of the Au electrode modified by Zn as the anode electrocatalyst of direct borohydride fuel cell, Int. J. Hydrogen Energy 36 (2011) 8857–8863, https://doi.org/10.1016/j.ijhydene.2011.04.128.
[76] C.C. Iyigun Karadag, G. Behmenyar, F.G. Boyaci San, T. Şener, Investigation of carbon supported nanostructured PtAu alloy as electrocatalyst for direct borohydride fuel cell, Fuel Cell. 15 (2015) 262–269, https://doi.org/10.1002/fuce.201300060.